Electronic Supplementary Information (ESI) for

Ultrathin RhCo nanowires with defect-rich active sites for alkaline hydrogen evolution electrocatalysis

Luyu Zhu,[1] Dongdong Xu,[2,*] and Chenglin Yi[1,*]

[1]Key Laboratory of Green Chemistry and Technology of Ministry of Education, College of Chemistry, Sichuan University, Chengdu 610064, China. E-mail: clyi@scu.edu.cn

[2]Jiangsu Key Laboratory of New Power Batteries, Jiangsu Collaborative Innovation Center of Biomedical Functional Materials, School of Chemistry and Materials Science, Nanjing Normal University, Nanjing 210023, China. E-mail: ddxu@njnu.edu.cn

Experimental Sections

Chemicals and materials

Rhodium chloride hydrate (H_3RhCl_6), cobalt nitrate ($Co(NO_3)_2$), iron nitrate ($Fe(NO_3)_2$), nickel nitrate ($Ni(NO_3)_2$), copper nitrate ($Cu(NO_3)_2$), zinc nitrate ($Zn(NO_3)_2$), dioctadecyldimethylammonium chloride (DODAC), cetyltrimethylammonium chloride (CTAC), L-ascorbic acid (AA), sodium borohydride ($NaBH_4$), hydrazine (N_2H_4), and commercial palladium carbon (Pd/C) were purchased from Alfa Aesar. Sodium hydroxide (NaOH), hydrochloric acid (HCl), and ethanol were obtained from Sinopharm Chemical Reagent Co. Ltd. Docosyltrimethylammonium chloride ($C_{22}TAC$) was synthesized following the procedures in our previous report (*Chem. Sci.,* 2018, 9, 4451). All above reagents were utilized without further purification with analytical reagent grade.

Synthesis of RhCo NWs and corresponding electrocatalysts

Ultrathin RhCo alloy NWs were prepared by a nanoconfined attachment route in an aqueous solution with DODAC as the template, H_3RhCl_6 and $Co(NO_3)_2$ as the metal precursors, and $NaBH_4$ as the reducing agent. In a typical synthesis, 15.0 mg of DODAC was first dissolved in 5.0 mL of deionized H_2O to obtain a homogeneous solution at 75 °C. After cooling down to room temperature, 0.50 mL of HCl (200 mM), 0.40 mL of H_3RhCl_6 solution (10 mM) and 0.20 mL of $Co(NO_3)_2$ (10mM) were added into the surfactant solution. The solution was kept static at 25 °C for 30 min. Then, 0.50 mL of freshly prepared $NaBH_4$ (0.13 M) was injected into above solution. After being reacted for 2 h, RhCo NWs were collected by centrifugation and further washed several times with ethanol/H_2O. Similarly, RhFe NWs, RhNi NWs, RhCu NWs, and RhZn NWs were prepared by the similar procedures but having different metal precursors of $Fe(NO_3)_3$, $Ni(NO_3)_2$, $Cu(NO_3)_2$, and $Zn(NO_3)_2$. Besides, monometallic Rh NWs were prepared by similar processes with $RhCl_3$ as the sole metal precursor.

Electrochemical hydrogen evolution reaction (HER) test

The electrocatalytic tests were performed on the CHI 660E electrochemical analyzer as reported in our previous work (*Small* 2023, 202208077; *Adv. Funct. Mater.* 2022, 32, 2208057). A three-electrodes system was used for all electrochemical tests (a carbon rod as the counter electrode, a silver/silver chloride electrode (SCE) as the reference electrode, and RhCo NWs coated onto glassy carbon electrode (GCE, 0.07065 cm^2) as the working electrode). A well-dispersed suspension of catalyst was

prepared by mixed solution of 1.0 mg nanocatalysts, 4.0 mg of Valcan XC-72, and 2.0 mL ethanol/ H_2O (1:3). Then, 25 μL of Nafion solution (5.0 wt. %) was added and further treated under ultrasonic treatment for another 30 min. 6.0 μL above-prepared catalysts ink was coated onto pre-treated GCE and dried before the electrocatalytic tests. Note: The Ag/AgCl electrode should be fresh and maintain in saturated KCl solution after the test immediately

Characterizations

Mesoscopic morphology and atomic crystallographic structure were characterized on a JEM-F200 transmission electron microscope (TEM) operated at 200 kV. Elemental mappings were collected on FEI Talos F200X apparatuses at an accelerating voltage of 200 kV (high-angle annular dark-field scanning TEM (HAADF-STEM)). Crystallographic structure was also studied with X-ray diffraction (XRD) on powder samples using a D/max 2500 VL/PC diffractometer (Japan) equipped with graphite-monochromatized Cu Kα radiation. Surface electronic states were performed on a scanning X-ray microprobe (Thermo ESCALAB 250Xi) under Al Kα radiation (X-ray photoelectron spectra (XPS)). Inductively coupled plasma mass spectrometry (ICP-MS) was tested on a NexION 350D.
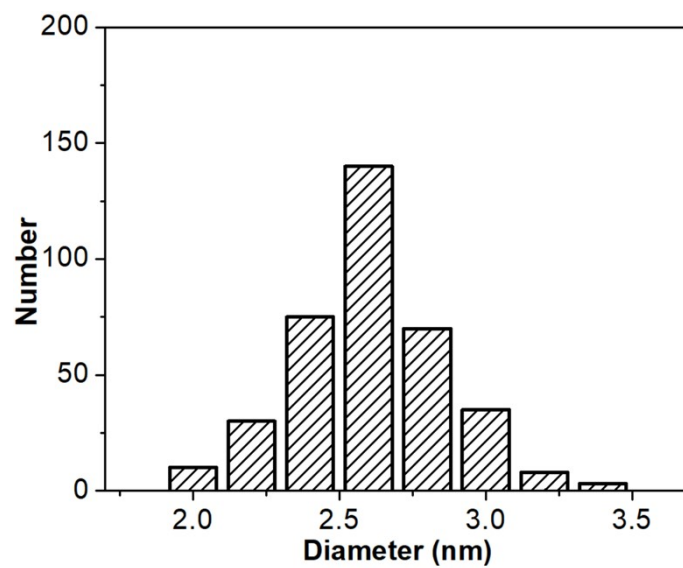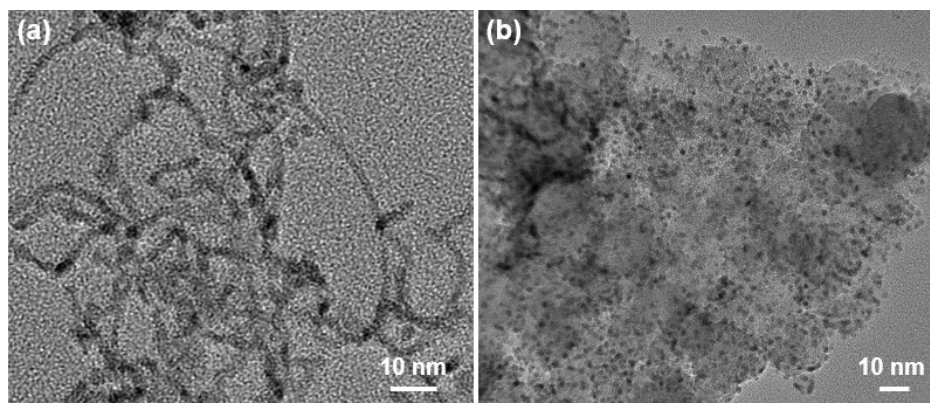
Fig. S1 Average diameter of one-dimensional RhCo NWs summarized from ~400 samples.
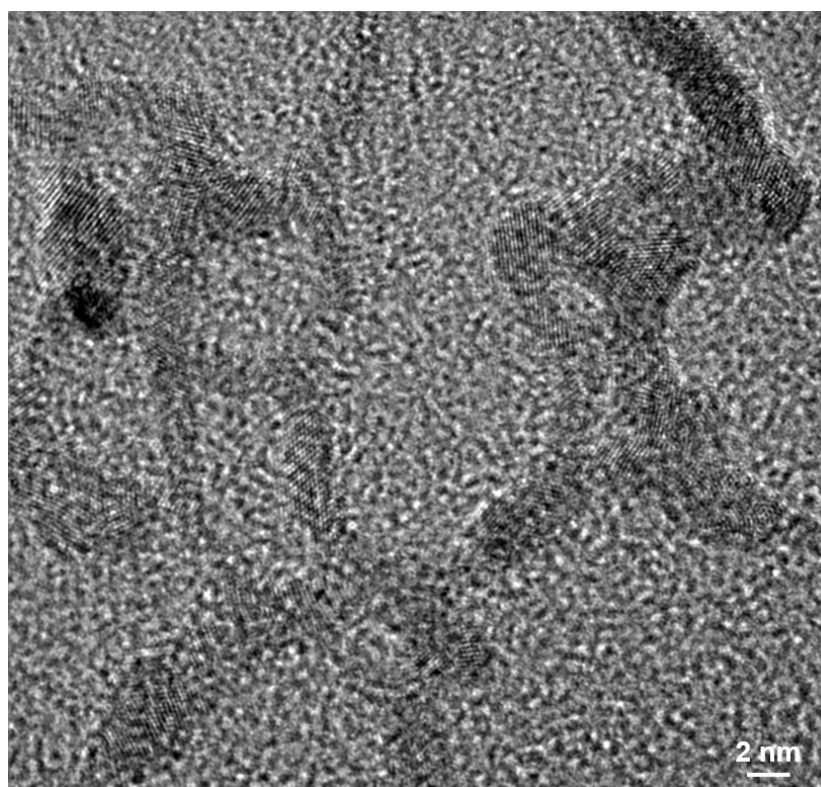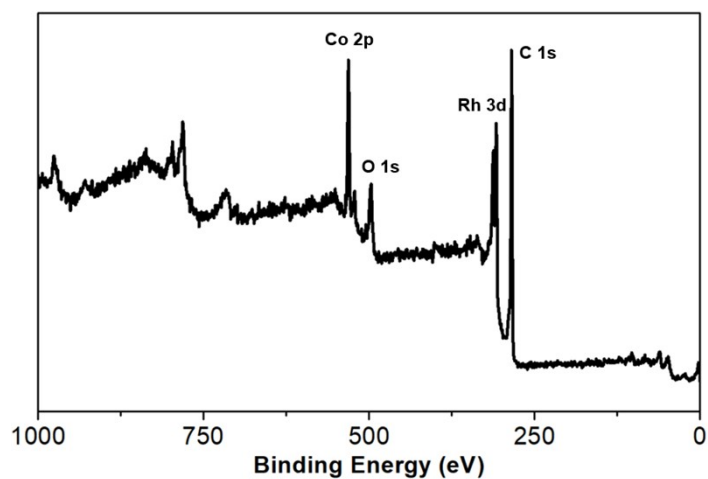

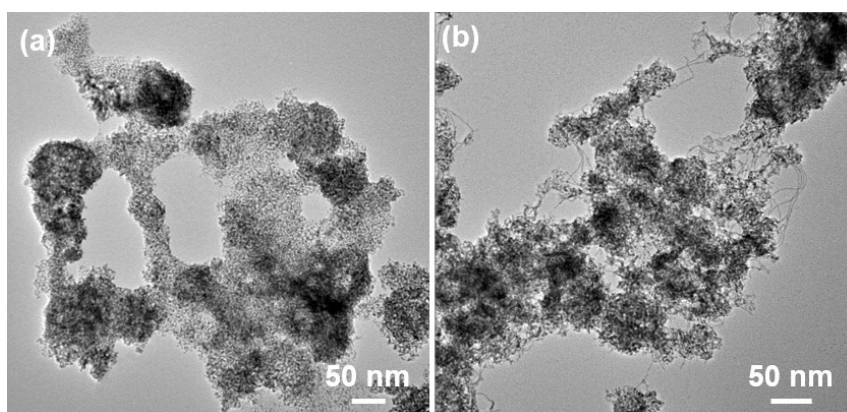**Fig. S2** High-resolution TEM image of one-dimensional RhCo NWs.
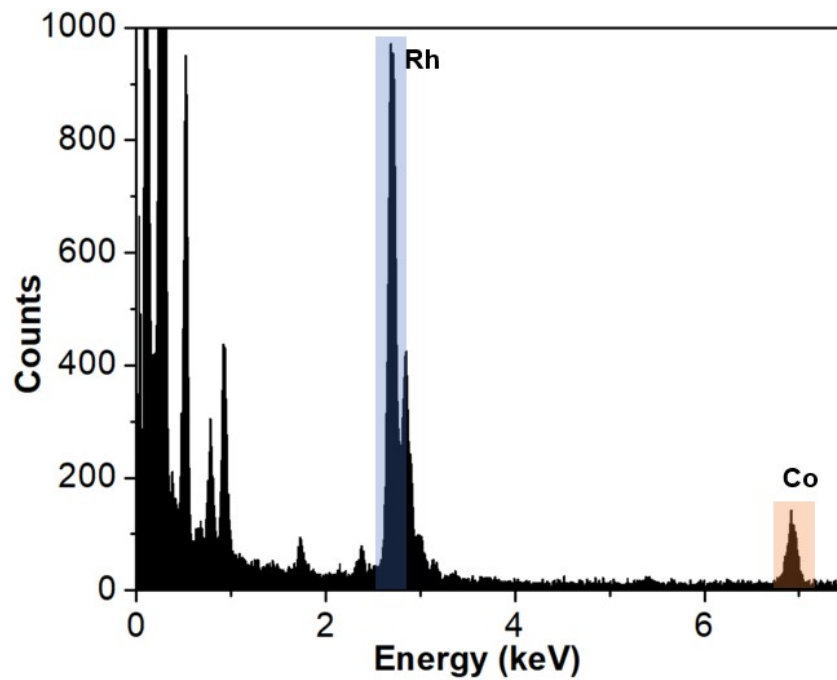
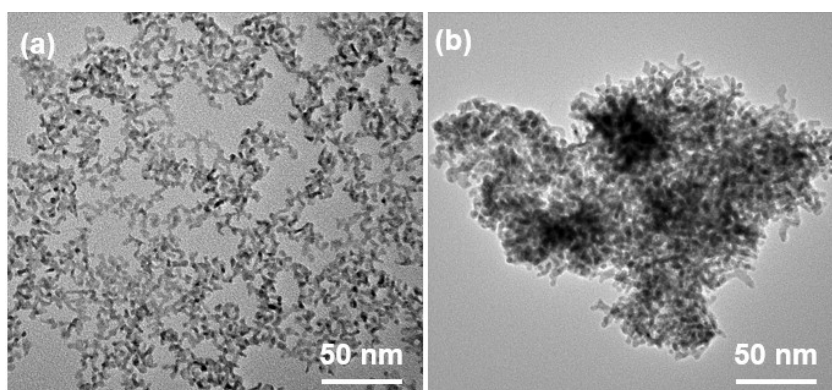**Fig. S3** HAADF-STEM EDS spectra of one-dimensional RhCo NWs.

Fig. S4 TEM images of (a) one-dimensional Rh NWs and (b) bimetallic RhCo NPs.
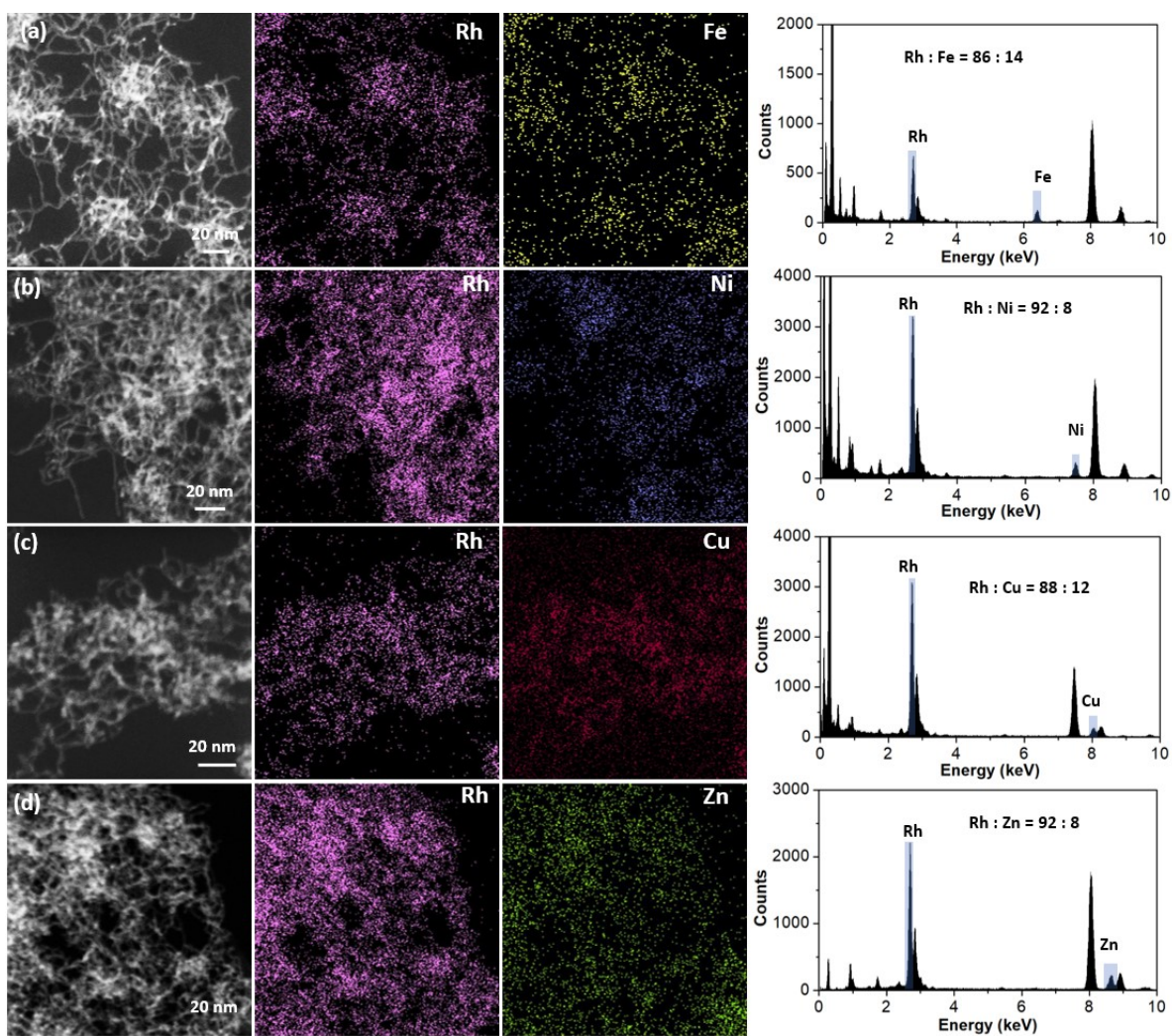
**Fig. S5** XPS survey spectrum of RhCo NWs.

Fig. S6 TEM images of RhCo nanostructures synthesized under (a) lower and (b) higher pH of reaction solution.


Fig. S7 TEM images of RhCo nanostructures synthesized under (a) lower and (b) higher temperatures of reaction solution.

Fig. S8 HAADF-STEM images and corresponding EDS mapping spectra of (a) RhFe NWs, (b) RhNi NWs, (c) RhCu NWs, and (d) RhZn NWs. Note: carbon coated Cu TEM grid was used for RhFe, RhNi, and RhZn NWs, while carbon coated Ni TEM grid was used for RhCu NWs.
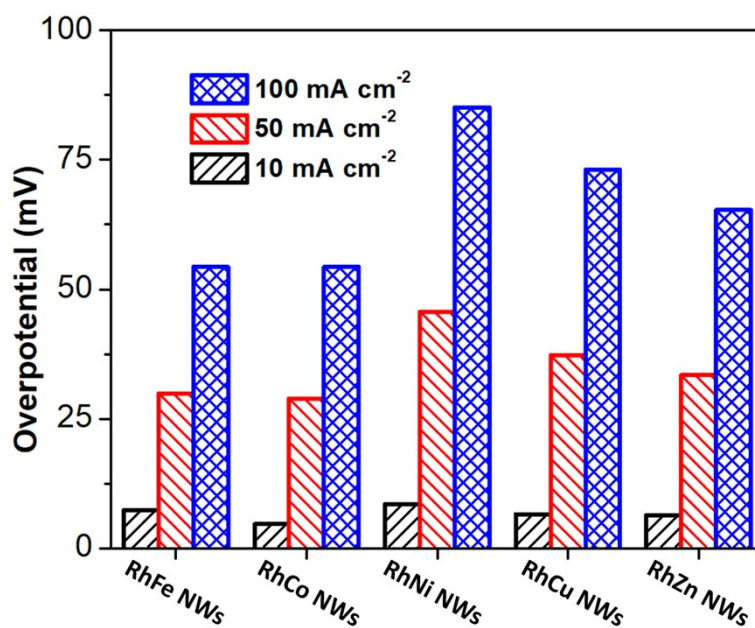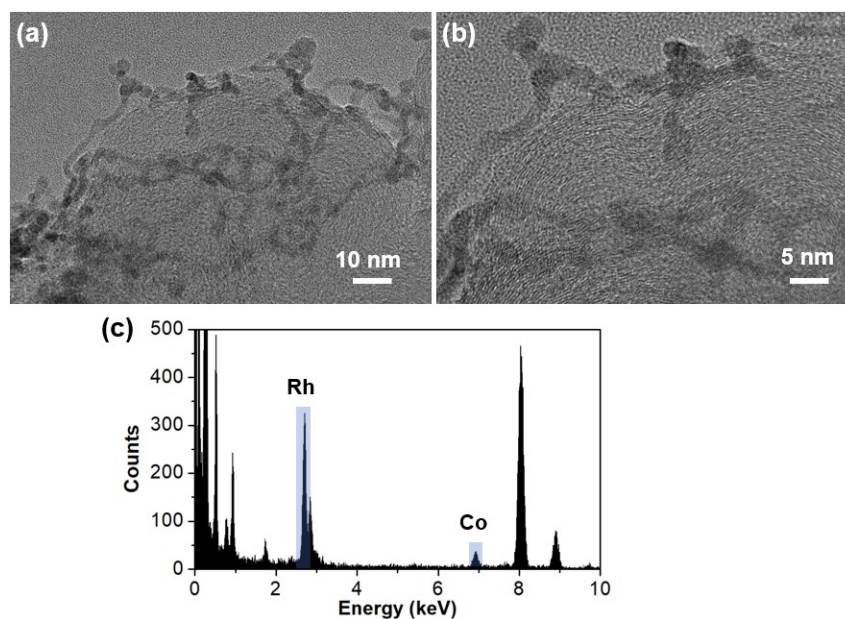
Fig. S9 Summarized overpotentials of one-dimensional RhM alloy NWs collected from Fig. 4a.
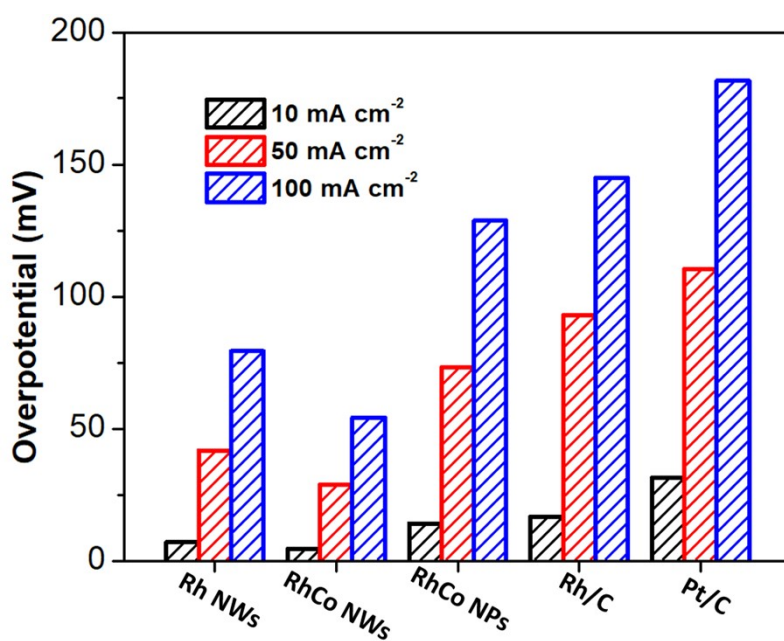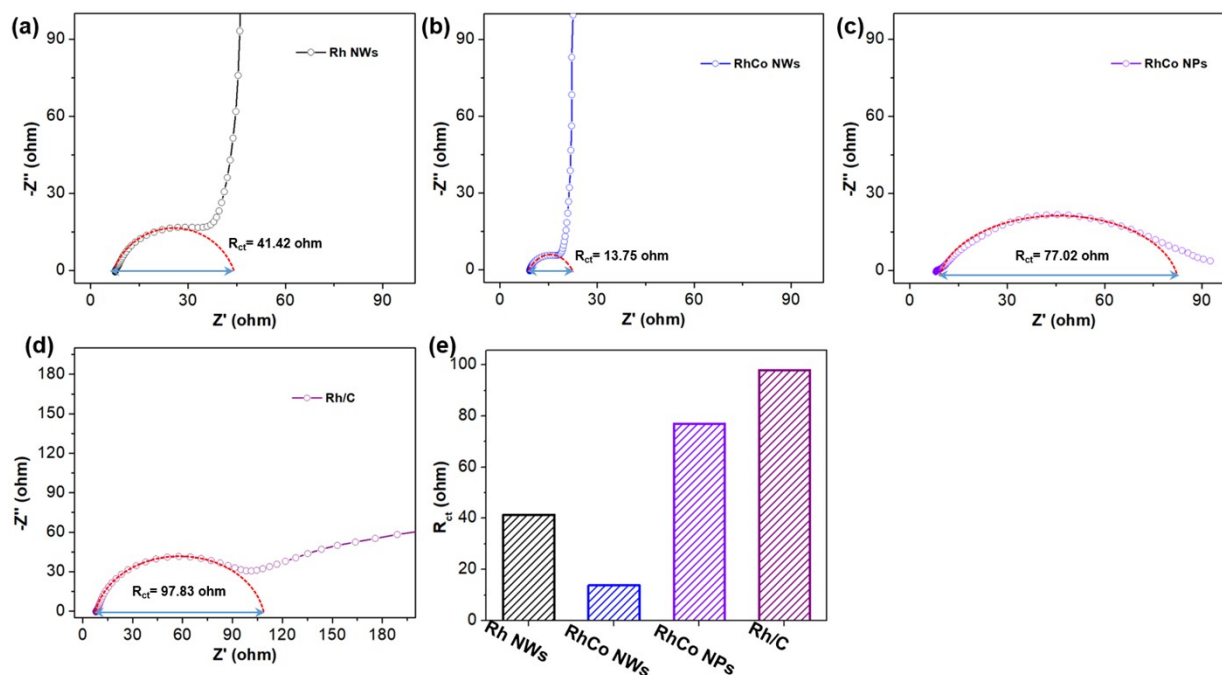

Fig. S10 Summarized overpotentials of Rh NWs, RhCo NWs, RhCo NPs, Rh/C, and Pt/C collected from Fig. 4b.

Fig. S11 (a, b) TEM images and (c) corresponding EDS spectrum of RhCo NWs collected after HER electrocatalysis.

**Fig. S12** The R_{ct} value of (a) Rh NWs, (b) RhCo NWs, (c) RhCo NPs, and (d) Rh/C. (e) Summarized R_{ct} values of Rh NWs, RhCo NWs, RhCo NPs, and Rh/C.

Note for Fig. S12: The R_{ct} of RhCo NWs and Rh NWs were deeply lower than RhCo NPs and Rh/C, which indicated that the bigger aspect ratio of nanowires would accelerate the formation of a percolation network and facilitated the electron transfer.
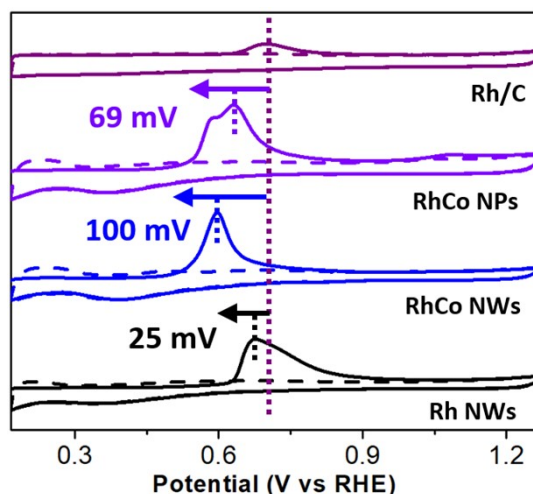
Fig. S13 Electrochemical CO stripping plots of Rh NWs, RhCo NWs, RhCo NPs, and Rh/C.
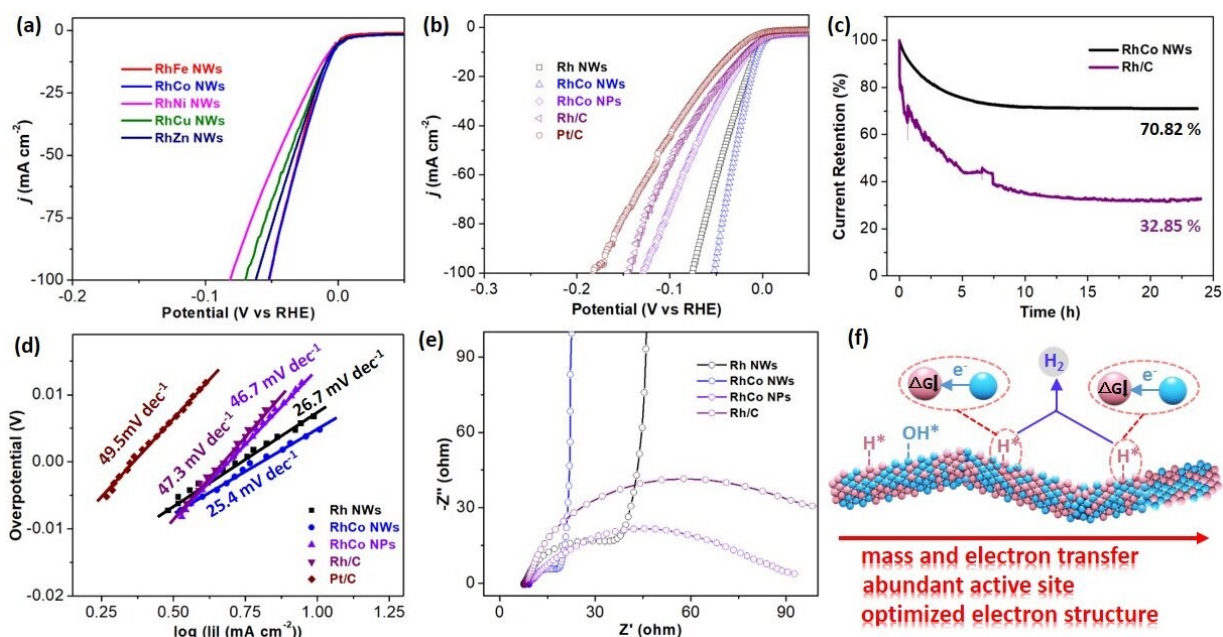
Fig. S14 Enlarged Fig. 4 showed in the Manuscript. (a) LSV curves of RhM alloy NWs collected in N_2-saturated 1.0 M KOH. (b) LSV curves and (c) chronoamperometry stability of RhCo NWs and corresponding counterpart electrocatalysts collected in N_2-saturated 1.0 M KOH. (d) Tafel plots and (e) EIS curves of Rh NWs, RhCo NWs, RhCo NPs, and Rh/C. (f) Schematic illustration of high activity of RhCo NWs in HER electrocatalysis

Table R1. Comparison of electrocatalytic HER performance of our electrocatalysts and some recently reported counterparts in alkaline electrolytes.

Catalyst	Loaded Catalysts Amount (mg cm^{-2})	Current Density (mA cm^{-2})	Overpotential (mV)	Reference
Rh NWs	0.042	10	7.37	This work
RhCo NWs	0.042	10	4.62	This work
Rh NSs	0.017	10	37.8	*Sci. Adv.* **2021**, *7*, eabd6647
w-Rh$_2$P NS/C	0.0123	10	18.3	*Adv. Energy Mater.* **2018**, *8*, 1801891
Rh/RhO$_2$ nanoparticle	0.20	10	14	*Adv. Mater.* **2020**, *32*, 1908521
P-Rh	0.022	10	20	*J. Mater. Chem. A* **2020**, *8*, 11923
Rh-Rh$_2$P@C	0.0142	10	37	*J. Mater. Chem. A* **2020**, *8*, 12378
Ir$_{0.7}$Rh$_{0.3}$Sb	0.35	10	22	*Adv. Energy Mater.* **2022**, *12*, 2200855
Pt NWs/SL-Ni(OH)$_2$	0.016	4	85.5	*Nat. Commun.* **2015**, *6*, 6430
Pt$_3$Ni$_2$-NWs-S/C	0.015	10	42	*Nat. Commun.* **2017**, *8*, 14580
Pt$_1$/N-C	0.25	10	46	*Nat. Commun.* **2020**, *11*, 1029
PtSn$_4$ single crystal	-	10	37	*Angew. Chem. Int. Ed.* **2019**, *58*, 13107